An Object-Based Classification Approach in Mapping Tree Mortality Using High Spatial Resolution Imagery

Qinghua Guo[1]
School of Engineering, University of California at Merced, P.O. Box 2039, Merced, California 95344

Maggi Kelly and Peng Gong
Department of Environmental Science, Policy, and Management, 137 Mulford Hall #3114, University of California, Berkeley, California 94720-3114

Desheng Liu
Department of Geography, The Ohio State University 1036 Derby Hall, 154 North Oval Mall, Columbus, Ohio 43210-1361

Abstract: In California, a newly discovered virulent pathogen (*Phytophthora ramorum*) has killed thousands of trees, including tanoak (*Lithocarpus densiflorus*), coast live oak (*Quercus agrifolia*), and black oak (*Quercus kelloggii*). Mapping the distribution of overstory mortality associated with the pathogen is an important part of disease management. In this study, we developed an object-based approach, including an image segmentation process and a knowledge-based classifier, to detect individual tree mortality in imagery of 1 m spatial resolution. The combined segmentation and classification methods provided an easy and intuitive way to incorporate human knowledge into the classification process. The object-based approach significantly outperformed a pixel-based maximum likelihood classification method in mapping the tree mortality on high-spatial-resolution multispectral imagery.

INTRODUCTION

In many coastal forests of central California, a newly discovered virulent pathogen (*Phytophthora ramorum*) has killed hundreds of thousands of trees, including tanoak (*Lithocarpus densiflorus*), coast live oak (*Quercus agrifolia*), and black oak (*Quercus kelloggii*) (Rizzo and Garbelloto, 2003). This phenomenon is commonly referred to as "Sudden Oak Death" (SOD), and it has reached epidemic levels in several areas of the state (Garbelotto et al. 2001; Rizzo et al. 2002). Monitoring this

[1]Corresponding author; email: qguo@ucmerced.edu

GIScience & Remote Sensing, 2007, **44**, No. 1, p. 24–47.

disease through time is critical for management and for further elucidating disease spread patterns through time (Kelly and McPherson, 2001).

Landscape pathology is an emerging field that seeks to understand the establishment, spread, and impact of forest diseases as a consequence of the interaction between spatial heterogeneity of the environment, landscape structure, and population dynamics of the pathogen (Holdenrieder et al., 2004). To this end, technologies such as remote sensing and geographic information systems (GIS) are valuable tools to monitor the spatial components of disease across scales. Moderate– to large–spatial resolution imagery (10–30 m) has been used to derive forest structure and health (Boyer et al. 1988; Muchoney and Haack 1994; Everitt et al. 1999); however, mapping individual tree crowns necessitates the use of spatial resolutions smaller than an individual tree. Indeed, the application of high spatial resolution imagery to map individual trees is a new and growing area of research. For example, several researchers have recently used high spatial resolution imagery to study the demographic characteristics (size, location, mortality, and growth) of individual trees in the tropical rain forest in Brazil (Read, 2003; Clark et al. 2004). They found the imagery very useful for monitoring individual trees through time in a consistent manner.

Our research goals are similar to others mapping individual trees: we seek to monitor individual trees through time, which could aid in studying the landscape-scale patterning of the mortality in order to understand the landscape pathology of the establishment and spread of SOD. This new disease has characteristics that make remote sensing using high spatial resolution imagery an appropriate choice for monitoring (Kelly et al., 2004a). First, the affected trees are large (≥3 m diameter) and comprise the forest overstory, and second, in most cases, as the trees with the disease die the entire crown changes dramatically from healthy green to brown over a short time period (Rizzo and Garbelotto, 2003). Despite these dramatic visual characteristics associated with the disease, conventional pixel-based classification (e.g., maximum likelihood classifiers) of tree mortality from high-spatial resolution (e.g., 1 m) remotely sensed imagery have not produced operationally satisfactory results (Kelly et al., 2004). This is due to the high local spectral variability from individual trees (high-spatial resolution imagery integrates branches, shadows, and leaves into each pixel, providing a complex locally variable radiance signature across an individual tree) (Wulder et al., 2004).

During the past decades, high-spatial-resolution remotely sensed images have become commercially available and increasingly used in various aspects of environmental monitoring and management (Treitz et al., 1992; Mumby and Edwards, 2002). Conventional pixel-based classifiers such as maximum likelihood classification (MLC) and Iterative Self-Organizing Data Analysis Technique (ISODATA), which label unknown areas pixel by pixel based on spectral similarity, do not perform well with high-spatial-resolution images (Toll, 1984; Xia, 1996). This is because the inherent spectral variability in specific ground targets increases as resolution becomes finer (Martin and Howarth 1989). Although efforts have been made to incorporate texture and contextual information for pixel-based classifiers to improve classification accuracies (Gong and Howarth, 1990b, 1992; Sali and Wolfson, 1992; Karathanassi et al., 2000; Debeir et al., 2002; Liu et al. 2006), pixel-based classifiers have difficulty in incorporating information such as spatial shapes and topology into the classification

process, and per-pixel classification of discrete features such as trees often result in considerable speckle (Kelly et al., 2004).

For these reasons, experienced photointerpreters often outperform computer algorithms in interpreting high-spatial-resolution imagery, and manual classification results are used as reference data for comparisons with computer algorithms (Brandtberg and Walter, 1998). Despite the fact that the human eye is less capable of differentiating between levels of grey than computer algorithms, the power of the human brain in image interpretation comes from our ability to make inferences based not only on spectral properties, but also on information such as object shape, texture, and spatial relationships, as well as human knowledge (Biederman, 1987). Land cover/land use types that are confusing for computer algorithms can be easily identified by humans. For example, a building and a road in an image can be spectrally similar, and consequently difficult for computer algorithms to distinguish between. However, photointerpreters can easily distinguish between these features based on knowledge about object shapes. Humans tend to delineate images into homogenous areas, and then interpret the images via domain knowledge (Gong and Howarth 1990a; Laliberte et al., 2004). To approximate the image interpretation ability of humans, we developed a hybrid method that combined object-based and knowledge-based classifications to detect tree mortality associated with SOD using high-spatial-resolution imagery.

Researchers have demonstrated that knowledge-based classification methods are able to incorporate human knowledge into classifiers and improve classification accuracies. Human knowledge can be expressed in several ways for the use of knowledge-based classifiers (Binaghi et al., 1997; Murai and Omatu, 1997). For example, the simplest, and commonly used approach is rule-based (also referred to as production rules; Richards and Jia, 1999). Examples of application of knowledge-based classification methods are follows. Bardossy and Samaniego (2002) applied a fuzzy rule–based method to classify Landsat Thematic Mapper (TM) imagery in southern Germany: their fuzzy classification algorithm utilized a rule system derived from a training set. Harris and Ventura (1995) used zoning and housing density data to post classify the initial maximum likelihood classification results of TM data. Stefanov et al. (2001) performed post classification sorting of initial land cover classification using ancillary data such as texture, land use, and water rights. Murai and Omatu (1997) believed that humans classified remotely sensed images not only by the focal pixel but also by using the neighboring pixels. Therefore, they proposed a knowledge-based post classification sorting of land cover classification results from TM data using texture information derived from a 3×3 pixel filter template, which consisted of both the target pixel and its nearest eight neighboring pixels. However, a filter template is limited in its capacity to represent more sophisticated spatial relationships or geometry of objects (e.g. shapes and proximity) (Gong and Howarth, 1990a). An obvious extension of these examples is to apply knowledge-based methods to classify image objects. In contrast to pixel-based classifiers, object-based classifiers first segment an image into homogeneous objects, in which neighboring spectrally similar pixels are grouped together to form an object (Baraldi and Parmiggiani, 1996; Tremeau and Borel, 1997; Hay et al., 2001); then clustering methods are applied to classify the objects based on features (e.g., spectral and spatial properties) extracted from the objects.

The objective of this study was to evaluate the effectiveness of a hybrid classification method that combined object-based and knowledge-based classification methods to map the disease-related tree crown mortality using high-spatial-resolution remotely sensed imagery. We first described a modified region-based segmentation method and algorithms to extract both spectral and spatial information from segmented images. We also discussed limits of a commonly used shape index, and proposed a relative shape index. Finally, we applied the proposed method to detect dead crowns in our study area, and the result was compared to the conventional pixel-based maximum likelihood method.

STUDY AREA AND REMOTELY SENSED DATA

Our study area, China Camp State Park (CCSP) in Marin County (122°29', 38°00'), is a wooded peninsula on San Pablo Bay, and is considered to be a "hot spot" for SOD (Svihra, 1999). The area has moderate to steep topography, with elevations ranging from sea level to over 300 m. The forest stands are near even-age stands, as these hillsides were harvested for timber in the early to mid-1800s. Coast live (*Quercus agrifolia*), black (*Quercus kelloggii*), and valley oaks (*Quercus lobata*) are abundant, and occur in mixed stands with mature madrone (*Arbutus menziesii*) and California bay (*Umbellularia californica*). While all of these trees with the exception of valley oak are hosts for *P. ramorum,* coast live and black oaks are the targets for this project as they are the only hosts that show the dramatic canopy color changes described earlier. The other species mentioned are defined as "foliar hosts," meaning that the pathogen usually attacks their leaves, instead of causing the more extensive trunk cankers found on the *Quercus* individuals (Rizzo et al., 2002). These species are also important in inoculum build-up and dispersal throughout the forest (Kelly and Meentemeyer, 2002; Rizzo and Garbelotto, 2003). In this work, we attempt to distinguish dead individuals from the two target tree species from bare areas and the surrounding forest mosaic via the hybrid algorithm. We located a 5 ha rectangular-shaped forested area, 20 m above sea level, and ground-truthed (via GPS and hard copy imagery) all dead stems found therein. Digital imagery (Airborne Data Acquisition and Registration, ADAR) was acquired for the larger CCSP area on May 5, 2001 with an ADAR 5500 imaging system that was comprised of a 20 mm lens with four mounted cameras (spectral bands: blue: 450–550 nm, green: 520–610 nm, red: 610–700 nm, near infrared [NIR]: 780–920 nm). Imagery was acquired near noon, in clear-sky conditions (solar elevation = 58.65°). We contracted with a private company (Positive Systems, Inc. from Montana) to perform the imagery acquisition and registration. RMS error was reported to be less than 1 m. The average ground spatial resolution of the images is 1 meter. Each 1,000 × 1,500 m frame was captured with 35% end- and 35% sidelap. Further information about the imagery can be found in Kelly et al. (2004a).

METHODS

The object-based classification involved the following steps (Fig. 1). First, we segmented the ADAR image into "objects." Second, spectral content, object geometry, and topological relations among objects were extracted. Third, knowledge-based spatial

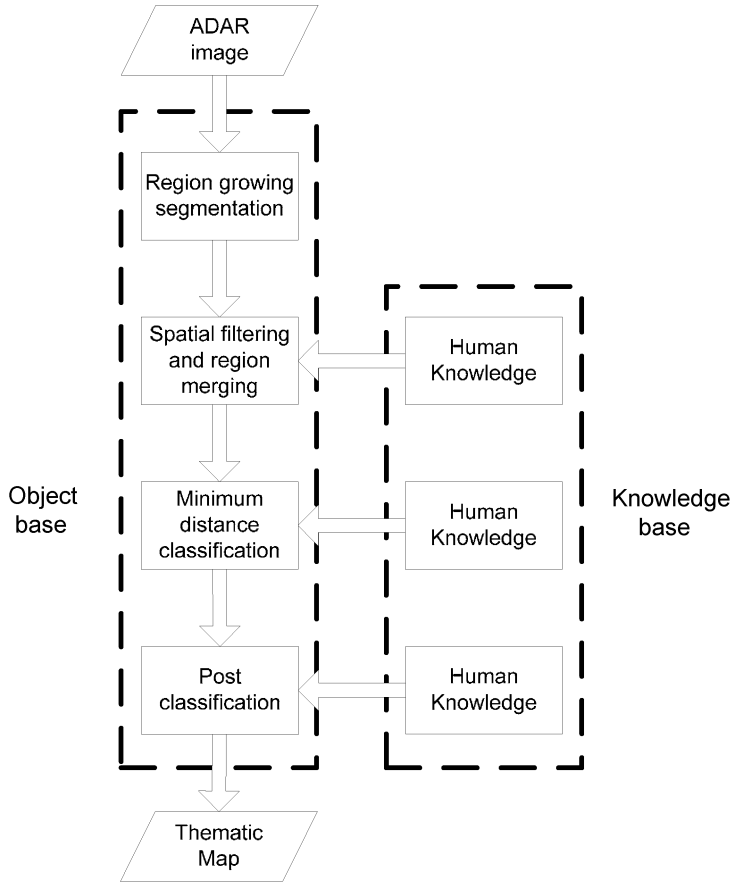

Fig. 1. Flow chart of the hybrid method combining objected-based and knowledge-based classifications. The left panel represents the object based classification methods, and the right panel the incorporation of human knowledge into object-based methods. A rule-based approach is used to represent human knowledge in the classification.

merging and filtering were applied to eliminate small and irregular objects. Finally, a minumum distance classifier together with a knowledge-based post-classification method were performed. We then classified the image using a maximum likelihood classifier (MLC). Finally, the accuracies of the proposed method and the MLC method were compared.

Image Segmentation

An "object" is defined here as a group of spectrally similar contiguous pixels, and ideally, it should represent a physically or ecologically homogeneous land class. Numerous algorithms have been proposed to generate segmented images. They fall into two broad classes: edge-based methods or region-growing methods. For multi-spectral imagery (like the ADAR imagery used in this study), it is relatively difficult to compute the gradient of the vector field to obtain edges of the image in edge-based

methods (Cumani, 1991; Li and Narayanan, 2003). Therefore, we used a region-growing method, which is a simple and popular segmentation method. Unlike edge-based methods, the region-growing method can produce closed regions. Another advantage of this method is that it is flexible in handling multi-spectral data and is able to utilize different similarity criteria. One possible drawback of the method is that the region-growing method potentially generates a segmented image with many small regions (objects). Consequently, a merging procedure is usually applied after the initial segmentation. We modified the single-linkage region-growing algorithm (SLRG) (Baraldi and Parmiggiani, 1996) to address some of the limitations of the region-growing method used in this study (e.g., lack of local adaptability) by combining multiple homogeneity criteria. It should be noted that there is no universal segmentation method that could be used for all types of landscapes (Pal and Pal, 1993; Zhang and Luo, 2000; Hay et al., 2001; Carleer et al., 2005). In this study, we found that the proposed segmentation method was useful for separating dead tress from other ground types. However, the result did not exclude the use of other methods. For example, the commercially available software eCognition also implements a region growing technique (Baatz and Schape, 2000), which starts with a one-pixel object and interactively merges it into larger objects (Hay et al., 2005). Comparison among different segmentation methods is beyond the scope of this study; readers who are interested in more information about different segmentation algorithms may refer to Zhang (1997), Carleer et al. (2005), and Hay et al. (2001).

The segmentation method used in this study began when the procedure sequentially scanned an image. Any unlabeled pixel (i.e., a pixel that has not yet been assigned to any object) is used as a "seed" pixel that will grow into an object based on certain homogeneity criteria in either a four-connected or an eight-connected neighborhood**.** By visual inspection of the segmented image from these two methods, we found the four-connected neighborhood was more plausible in delineating shapes of dead crowns due to their relatively compact shapes. It should be noted that given the same threshold, the four-connected neighborhood method usually produces more conservative or restrictive shapes than the eight-connected neighborhood method. But the choice of neighbor connection types is case dependent and may depend on specific applications. For example, if the goal is to extract roads that are not horizontally or vertically distributed, the eight-connected neighborhood method may be more suitable. Moreover, tuning the homogeneity thresholds for four-connected and eight-connected neighborhood types could reduce the differences between them. For example, a greater homogeneity threshold (i.e. more restrictive region-growing parameter) of the eight-connected neighbor type could result in similar segmented images as those using the four-connected neighbor type with a smaller homogeneity threshold (i.e., less restrictive region-growing parameter).

Homogeneity Criteria

Homogeneity criteria determine whether a seed pixel's neighbors belong to the seed pixel's object. Conventional SLRG procedures lack local adaptability (Sarabi and Aggarwal 1981) because they apply a single absolute homogeneity threshold to all local area situations. The relative local interpixel contrast (Moghaddamzadeh and Bourbakis, 1997), which is used to measure grey-level difference between a growing

pixel and its neighbors, has more flexibility in detecting the local variation among different objects. In this study, we used three homogeneity criteria: (1) the absolute spectral distance between the adjacent pixel and a seed; (2) the absolute local spectral distance between two local neighboring pixels; and (3) the relative local difference (measured by R^2) between two neighboring pixels. Their definitions are described as follows:

Absolute spectral distance between the adjacent pixel and a seed:

$$H1 = \sum_{i=1}^{4} (b_{si} - b_{ni}), \tag{1}$$

where b_s and b_n denote the digital values for a seed pixel and its adjacent pixel, respectively, and i represents the individual spectral band for the four-band ADAR image.

The absolute local spectral distance between two neighboring pixels (one belongs to a known object, another is yet to be determined):

$$H2 = \sum_{i=1}^{4} (x_i - y_i)^2, \tag{2}$$

where x represents the digital value of a known region pixel, and y represents a neighbor of x whose regional affiliation is yet to be determined.

The relative local difference between two neighboring pixels (measured by R^2):

$$H3 = \frac{\left[\sum_{i=1}^{4} (x_i - \bar{x})(y_i - \bar{y})\right]^2}{\sum_{i=1}^{4} (x_i - \bar{x})^2 \sum_{i=1}^{4} (y_i - \bar{y})^2}, \tag{3}$$

H1 and *H2* are commonly used to measure the inter-pixel similarity, but the thresholds among different objects (or regions) can be varied. Therefore, it is more appropriate to define a relative local difference (*H3*), which is less dependent on the absolute value. An unlabeled pixel will be assigned to the same region number as its seed pixel only if all three homogeneity measures pass the pre-defined thresholds.

Feature Extraction

One reason to segment an image into homogeneous regions is to extract more ecologically or physically meaningful features from the resulting objects. For example, the geometric features and spatial relations of objects can be easily generated

from the segmented image. Features extracted in this study include: (1) spectral properties such as mean and standard deviation of different spectral bands for the objects; (2) geometric properties such as the area, perimeter, and shape index of the objects; and (3) spatial relationship properties such as the topological relationships of the objects. We developed tools to gather these features from objects, and to update the features if and when objects were merged. Note that some metrics such as area and perimeter of the objects could be extracted from either commercial software (e.g., AcrGIS) or freely available tools (e.g., Fragstats). However, it is important for us to develop a tool that could calculate them because: (1) those metrics are the integrated part of the proposed method; and (2) the new shape index we proposed below is not available in any existing software.

Mean and Standard Deviation. The mean (m) and the variance (s) of the object are defined as:

$$m = \left(\sum_{i=1}^{n} x_i \right) / n , \tag{4}$$

$$s = \frac{n\left(\sum x^2\right) - \left(\sum x\right)^2}{n^2}, \tag{5}$$

where x is the digital value for a pixel, and n is the number of pixels inside the object. Once these two statistics were computed, we did not need to keep all the digital values for the object in order to save the computational memory and facilitate computation efficiency (Kermad and Chehdi, 2002). In addition, it is important to update the mean and variance when two objects are merged in real-time fashion. We developed the following two equations:

On-line mean updating:

$$m' = \frac{n_1 m_1 + n_2 m_2}{n_1 + n_2}, \tag{6}$$

where m' represents the newly updated mean; n and m represent the number of pixels and the mean value of the object; and 1 and 2 represent two objects to be merged, respectively.

On-line variance updating:

$$s' = \frac{n_1 s_1 + n_2 s_2}{n_1 + n_2} + \frac{n_1 n_2 (m_1 - m_2)^2}{(n_1 + n_2)^2}, \tag{7}$$

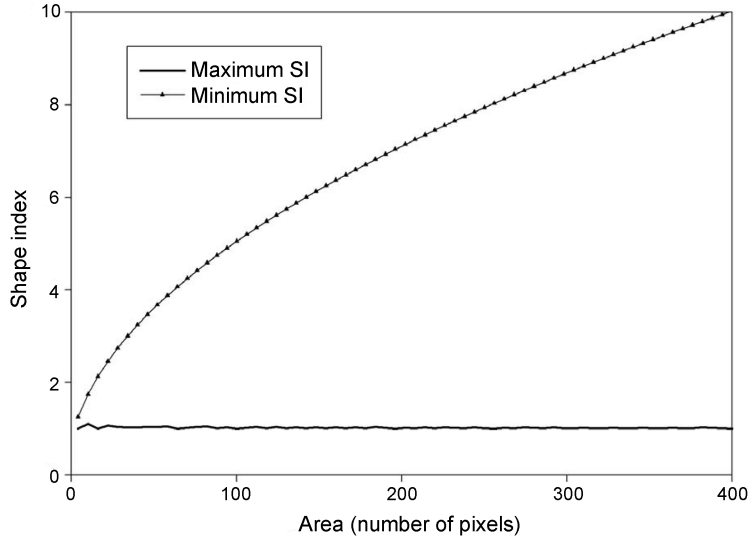

Fig. 2. Theoretical maximum and minimum values for the conventional shape index (*SI*) of given areas. The solid line represents the maximum SI given the size of an object, and the line with triangles represents the minimum SI given the size of an object.

where s' represents the new updated variance, and s_1 and s_2 represent the variance of two objects to be merged. A special case occurs when a growing object merges a single adjacent pixel. In such a case the above two equations can still be applied, simply by substituting $n_2 = 1$, $s_2 = 0$, and m_2 = the digital value of the adjacent pixel.

Geometric Properties. Acquiring and using object geometry (Xia, 1996; Li and Narayanan, 2003) has been shown to improve the performance of classification methods. We computed three basic properties of object geometry: area, perimeter, and a relative shape index. We felt that the shape index in particular would be useful in distinguishing dead crowns from bare areas, because the shapes of dead oak crowns are relatively compact. The conventional shape index (also called the compactness index, *SI*) is defined as:

$$SI = \frac{P}{4\sqrt{A}}, \tag{8}$$

where P and A are the perimeter and the area of an object, respectively. For raster data sets, a square is the most compact shape (*SI*=1). Researchers have used shape indices to assist in classification of imagery. For example, Xia (1996) applied the shape index together with a rule-based method to reduce the misclassification of an unsupervised classification map. In contrast, we found that comparisons of *SI* for different objects could be misleading since the components of the *SI* value are scale dependent, and vary with the area of an object. Figure 2 shows the change of maximum *SI* and minimum *SI* as the area of objects changes. The minimum *SI* is stable: regardless of the size of an object, the minimum *SI* stays close to 1. However, the maximum *SI* is sensitive to the area of an object. The larger the object is, the greater its potential maximum

SI. This makes comparison between *SI* for different objects complicated: such comparisons do not reveal actual edge complexity differences between objects. Therefore, instead of using absolute *SI*, we constructed a relative shape index (*RSI*):

$$RSI = \frac{SI - MinSI}{MaxSI - MinSI}, \tag{9}$$

where *MaxSI* and *MinSI* are the theoretical maximum and minimum shape indices, respectively. We developed the formula for computing theoretical maximum and minimum shape indices. For the four-connected neighbor, the theoretical maximum and minimum shape indices (*MaxSI* and *MinSI*) are calculated as following:

$$MinP = 4 \times Floor(\sqrt{A}) + 2 \times Ceiling\left(\frac{n - [Floor(\sqrt{A})]^2}{Floor(\sqrt{A})}\right), \tag{10}$$

$$MinSI = \frac{MinP}{4\sqrt{A}}, \tag{11}$$

$$MaxP = 2 \times A + 2, \tag{12}$$

$$MaxSI = \frac{MaxP}{4\sqrt{A}}, \tag{13}$$

where *MaxP* and *MinP* represent the theoretical maximum and minimum perimeters given the area of *A* of an object. Both A and P are pixel-based, rather than being the actual measurement. For example, one pixel has the area of 1 and the perimeter of 4. The Floor is the function which rounds a number down, toward zero, to the nearest non-decimal value (an integer or zero). Conversely, the Ceiling is the function which returns a number rounded up, away from zero, to the nearest non-decimal value. For example: Floor(0) = 0, Floor(0.3) = 0, Floor(0.7) = 0; Ceiling(0) = 0, Ceiling(0.3) = 1, Ceiling(0.7) = 1. Note that the *RSI* ranges from 0 to 1. The smaller the *RSI*, the more compact the object is. Figure 3 illustrated the comparison between *SI* and *RSI* for two objects with different areas. Figure 3B exhibited an elongated object with an area of 7 and a perimeter of 16, and Figure 3A showed a relatively compact object with an area of 73 and a perimeter of 52. By visual inspection of the objects A and B, it is evident that object B has a maximum irregular shape when using a 4-connected neighbor type, whereas object A, which is a dead crown, should have a relatively compact shape. Based on the *SI* value, we were not able to differentiate the shape differences between them (*SI*s for A and B are 1.52 and 1.51, respectively); however, when based on *RSI*, we clearly found that A (*RSI* = 0.14) was more compact than B (*RSI* = 1). *RSI* has the values ranging from 0–1, and 1 represents the most irregular shape for a given area. Therefore, *RSI* successfully showed that B was the most irregular shape for any object with an area of 7 pixels.

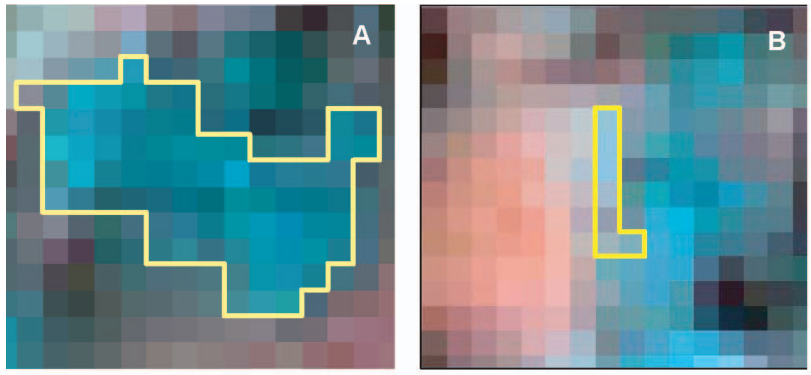

Fig. 3. Comparison between conventional shape index (*SI)* and relative shape index (*RSI)*.

Spatial Relationship Properties. Neighboring pixels tend to have similar spectral properties and are more likely to represent the same class. For pixel-based classifiers, researchers utilize contextual information to explore the spatial dependence structure among neighboring pixels (Gong and Howarth, 1992; Arbia et al., 1999; Solberg, 1999; Debeir et al., 2002). For object-based classifiers, the spatial dependence assumption for contextual classification methods is weakened due to the fact that pixels with similar reflectance are agglomerated to form a homogeneous object. Therefore, contextual classification methods are generally not suitable for object-based classifications (Steele and Redmond, 2001). However, the object-based classifiers offer other attractive properties—topological relations, which can be used to represent various aspects of sophisticated spatial dependence (or independence) structures. In addition, spatial topology can be easily incorporated into knowledge-based classifiers to improve classification accuracy (Tonjes et al., 1999). For example, if a linear object runs across the water, then the object is more likely to be a bridge than a road. For each object in the segmented image, we generated a unique polygon ID and stored them into two attribute tables, which were linked via the unique polygon ID. One table recorded the spectral properties such as mean and standard deviation of each band for an object, and the other table stored IDs of neighboring polygons for each object. The spatial topology information was then used in the knowledge-based classifiers described in the later sections.

Region Merging and Spatial Filtering. After initial segmentation by the region-growing method, the objects were extracted and feature properties were stored. As is typical with this method, our resultant map encountered two problems: (1) oversegmentation, in which a meaningful ground object is divided into several different polygons (Carleer et al., 2005); and (2) "salt-and-pepper" effects, where the segmented image contains too many scattered objects due to noise and detail (Tremeau and Borel, 1997) provided by the high-resolution imagery. Consequently, we applied region merging and spatial filtering to resolve these problems (Tremeau and Borel, 1997).

Spatial filtering was used to remove the "salt-and-pepper" effects on the segmented image using domain knowledge. From our field experience and visual inspection of the ADAR images, we know that the area of a dead crown is usually greater than four pixels, which can be successfully detected by ADAR images. Therefore, we

defined a speckle needing removal or merging to be any object whose area was less than or equal to four pixels, with one exception: a square object with four pixels was retained. A square with four pixels could be a small dead crown and is the minimum detectable unit for the dead tree in this study. Note that if and only if the object is a square, the relative shape index (RSI) equals 0. Consequently, we identified the speckle by setting the rules based on the area and *RSI*. For example, a non-square object with four pixels could be represented as "Area = 4" and "*RSI* > 0."

After identifying the speckle, we then merged it with other objects. One way to merge the speckle is based on the edges shared with its neighbors. The speckle is merged with the adjacent object with which it shares the greatest number of edges. In this study, we used the spectral similarity measured by R^2 between the speckle and its neighboring objects, because many of the speckles reside in the interiors of different objects or along the boundaries between them. It is reasonable to merge the speckle with the neighboring object having the greatest spectral similarity. Some practical issues also needed to be addressed. For example, if several speckles neighbor one another, an iterative pairwise maximum similarity algorithm was applied to avoid the order dependence. For example, if speckle B is considered to be speckle A's closest similar neighbor, and the similarity measure (R^2) between A and B passes the threshold, then if and only then is speckle A also considered to be speckle B's closest similar neighbor, and speckles A and B are merged. As noted, the process is iterative. The process will stop when no speckles can be found, or the program exceeds a user-specified maximum number of runs. The pseudo computer code of the spatial merging can be descried as follows:

```
If anObject.area < 4 or (anObject.area = 4 and anObject.RSI > 0) then
   aClosestNeighor = find_closest_similar_neighor(anObject)
   If aClosestNeighor.area > 4 or (aClosestNeighbor.area = 4 and
      aClosestNeighor.area.RSI = 0) then
         Merge(anObject, aClosestNeighbor)
   Else If anObject = find_closest_similar_neighor(aClosestNeighbor)
         Merge(anObject, aClosestNeighbor)

   End If
End if
```

After spatial filtering, we then applied a region-merging algorithm to combine adjacent objects that have similar spectral properties and belong to the same object from a human visual perspective. An R^2 calculation was used to evaluate the spectral similarity between two regions. Similar to spatial filtering, the iterative pairwise maximum similarity algorithm was used in the merging process.

Minimum Distance Classification and Knowledge-Based Classification. A minimum distance classifier was applied to classify the objects on the basis of their mean spectral reflectance. The shapes and spatial topology were used to construct the knowledge base to further improve the classification accuracies. Human knowledge can be expressed in several ways for the use of knowledge based classifiers (Binaghi et al., 1997; Murai and Omatu, 1997). The simplest, and commonly used approach is

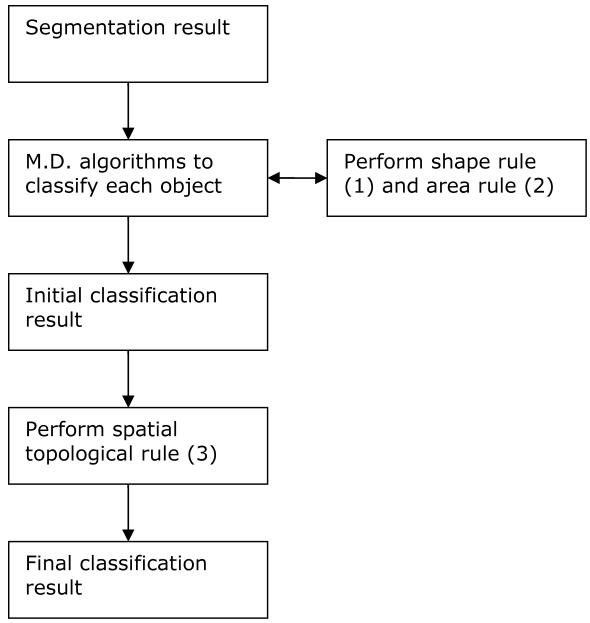

Fig. 4. Flow chart combining the minimum distance algorithm and the rule-based method. M.D algorithm = minimum distance classification method.

rule based (also referred to as production rules; Richards and Jia 1999), which takes the form of "If, Then" statements. Based on our field experience and ecological knowledge, as well as visual inspection of the ADAR images, we constructed the following three rules to improve our ability to distinguish dead crowns from other ground types (Fig. 4):

Rule 1 (area rule). No dead crowns have an area greater than 200 pixels. One of the major difficulties in detecting the dead crowns by automated computer algorithms involves the spectral confusion between the dead crowns and the bare areas. Conventional pixel-based classifiers have resulted in a significant amount of misclassifications between these two classes (Kelly et al., 2004, Liu et al., 2006). Yet the size of the objects can be used to aid in classifying dead crowns. For example, bare areas in this study area are often much larger than the dead crowns. From our field experience and visual inspection of the ADAR images, in the study area there are no dead crowns whose areas exceed 200 pixels.

Rule 2 (shape rule). Dead crowns have a relatively compact shape. The target dead trees are black oak and coast live oak, which have a relatively compact and round shape on remotely sensed images. We thus assumed that any irregular shape of a dead crown was mainly due to misclassification. Consequently, we applied the relative shape index to filter out those misclassification results. The threshold of RSI was determined by a trial and error method.

Rule 3 (spatial topology rule). Dead crowns must be adjacent to vegetation. Spread of the SOD relies on proximity of foliar hosts to target trees (Kelly and Meentemeyer, 2002; Rizzo et al., 2002). Based on these sources, and our field experience, we assume that all dead crowns are contained within the forest mosaic in the study

area. Consequently, if a classifier detects a dead crown that is isolated from vegetation (e.g., completely surrounded by water and bare areas), it is likely misclassified.

It should be noted that rule 1 and rule 2 were integrated into the minimum distance classification process, while rule 3 was used to post-classify the initial classified map because rule 3 relied on the completely mapped result to construct a spatial topology. We implemented the procedure as follows. First, we implemented the minimum distance classification method to label each object in the segmented map; second, we applied rule 1 and rule 2 to determine if there were misclassifications of dead crowns. For example, if either rule 1 or rule 2 identified an object as the misclassified dead crown, then the object was reassigned to its second nearest class. The above procedures were iterated until all objects in the segmented image were classified. Finally, we used rule 3 to further constrain the spatial topology of the dead crowns. Note that the advantage of integrating the rules into the classification process is that it can prevent the merging between misclassified land types and correctly classified land types, and allows for the rules to pull them apart. For example, if a bare area is misclassified as a dead crown, the misclassified dead crown could potentially be merged with its neighboring true dead crowns. As a result, in the post-classification process it is difficult to differentiate misclassified classes from correctly classified ones. However, when integrating knowledge-based classifications into the minimum distance classification, we are able to correct the misclassified classes before they are merged with other classes.

Classification Systems and Accuracy Assessment. We evaluated two classification schemes. The first consisted of four classes—dead crowns, bare areas, healthy vegetation, and shade (Level 1)—and the second consisted of two classes only—dead crowns and everything else (Level 2). Two hundred eighty-two (282) reference samples were obtained in the field and via manual interpretation. Fifty percent (50%) of the reference samples were used for training, and the rest were used to evaluate the performance of the classification methods (Benediktsson and Kanellopoulos, 1999). Because mapping the dead trees is the main objective of this study, and the total area of dead trees only accounts for a small percentage of the study area, we collected more dead tree samples per ha than other ground types. The classification results were also compared with a commonly used pixel-based method—the maximum likelihood classifier (MLC). The parameters of MLC were obtained by the training data and implemented in ERDAS software (ERDAS, 1999). The overall accuracy and Kappa coefficient were calculated and used in the comparison. The Kappa coefficient has the advantage that it measures the actual agreement between the classified results and the reference data with consideration of random chance; *z*-scores were computed to test if the methods were significantly different (Congalton and Mead, 1983).

RESULTS

The initial segmentation resulted in 6,538 objects (Fig. 5A), and subsequent spatial filtering was applied to merge small and irregular objects. The resultant segmented map contained only 1,277 objects (Fig. 5B). The large number of small objects can be explained by the changes of lighting condition, topography, mixed pixels, or noise—all typical of high-spatial-resolution imagery. In addition, the homogeneity threshold also played an important role in balancing the minimum detectable

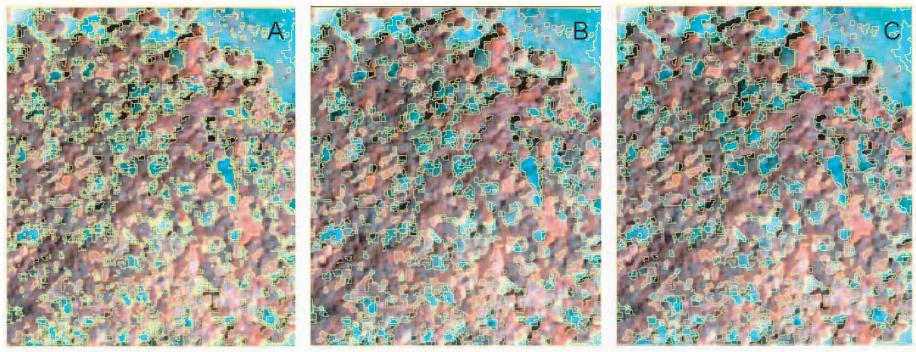

Fig. 5. Objects resulting from image segmentation, spatial filtering, and region merging. A. Initial segmentation with the region-growing algorithm, generating 6,538 objects. B. Resultant segmented image after spatial filtering, which generated 1,277 objects. C. Resulting segmented image after region merging, which generated 998 objects.

object and number of objects. We then conducted spatial merging to further merge the spectrally similar objects, resulting in 998 objects (Fig. 5C).

A minimum distance algorithm was applied to classify the final segmented image. Figure 6A shows the classification result overlaid with the reference dead trees. The minimum distance performed well in detecting the dead crowns (i.e., low omission errors). However at this stage, there were still a substantial number of commission errors due to misclassification of bare areas as "dead crown." We then imposed the knowledge-based classifier by integrating with the minimum distance classifier to post-classify the previous classification result. The knowledge-based classification greatly improved accuracies (Fig. 6B). For example, rule 1 (size limit) corrected region a in Figure 6A, rule 2 (compactness constrain) successfully removed dead crowns that were irregularly shaped (region c in Fig. 6A), and rule 3 (adjacency requirement) corrected some isolated pixels that were erroneously classified as dead crowns (region b in Fig. 6A). The results of the MLC method are shown in Figure 6C, which was fragmented and contained substantial confusion between dead crowns and bare areas.

The hybrid method combining object-based and knowledge-based classifiers was a great improvement over the MLC classifier for both classification schemes (Tables 1 and 2). For the more comprehensive classification scheme, the overall accuracies of the proposed method and MLC were 0.957% (kappa 0.930) and 0.716% (kappa 0.559), respectively. For the second scheme, the overall accuracies of the proposed method and MLC were 0.965 (kappa 0.929) and 0.865% (Kappa 0.729), respectively. The proposed method was significantly better than the MLC for both schemes at 95% confidence level (pairwise Z-scores of 6.263 and 3.037, respectively).

DISCUSSION

The modified single-linkage region-growing method was used to segment the image because the method can produce closed objects, and it is easy to incorporate multi-band information into the segmentation process. The method performed well in

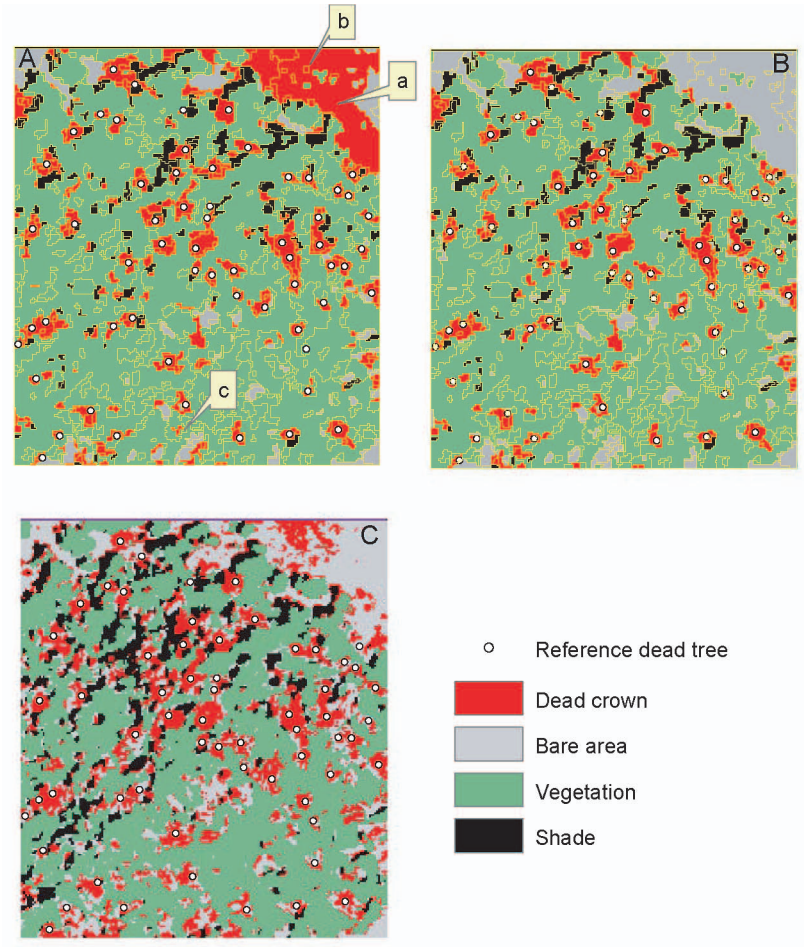

Fig. 6. Classification results using object-based methods and pixel-based methods. A. Object-based minimum distance classification. B. Object-based classification combining the minimum distance classifier and the knowledge-based classifier. C. Pixel-based maximum likelihood classification.

detecting dead crowns in our study on the basis of visual inspection and classification accuracies. However, it should be noted that our target objects are dead oaks, which in nature are relatively discrete and spectrally homogeneous, and have a compact shape in high-spatial-resolution images. There are more than a thousand segmentation algorithms available (Zhang and Gerbrands, 1994; Hay et al., 2003), and each of them has distinct theoretical backgrounds and uses different techniques. Many algorithms were developed for a specific use only, and it is believed that no single segmentation method can be applicable to all types of images (Pal and Pal, 1993; Zhang and Luo, 2000). Future research is needed to evaluate the performance of different segmentation algorithms on remotely sensed images from other areas.

After the region-growing segmentation process, the resultant segmented map still consisted of a large number of small objects ("salt-and-pepper" effects) due to the

Table 1. Error Matrices for the MLC Method and Hybrid Method Combining Object- and Knowledge-Based Classifications (OBKB)[1]

MLC method					
Classified as:	Dead	Bare	Vegetation	Shade	User's
Dead	66	5	5	0	0.868
Bare	8	8	10	0	0.308
Vegetation	0	1	19	0	0.950
Shade	1	0	10	8	0.421
Producer's	0.880	0.571	0.432	1.000	
				Overall	0.716
				Kappa	0.559
OBKB method					
Classified as:	Dead	Bare	Vegetation	Shade	User's
Dead	73	2	1	0	0.961
Bare	0	12	0	0	1.000
Vegetation	0	0	42	0	1.000
Shade	2	0	1	8	0.727
Producer's	0.973	0.857	0.955	1.000	
				Overall	0.957
				Kappa	0.930

[1]Level 1 classification system.

variation of local environmental conditions (e.g., light, topography) or errors (e.g., instrument failure). Lowering the homogeneity thresholds in the segmentation process will decrease the number of objects, however, because a small dead crown detectable from the ADAR image in our study could be as small as four pixels given a square shape. We chose to over-segment the image in order to prevent the merging of small dead crowns with other land types such as healthy forests and bare areas. A merging process that is guided by domain knowledge was then applied to remove the "salt-and-pepper" effects while retaining possible small dead crowns. For example, we merged any object whose area was less than or equal to four pixels, with the exception that a square object with four pixels was kept. A square object with 4 pixels could be represented as "Area = 4" and "RSI = 0."

We extracted both spectral and spatial information for each object of the segmented image. Spectral properties included mean and standard deviation of each band of an object, and spatial properties included area, perimeter, and spatial topology of an object. Based on the area and perimeter of an object, we derived a shape index, which is commonly used to characterize the edge complexity of a patch in landscape ecology. The shape index is also useful to improve classification actuaries (Xia, 1996). In this study, we found the conventional shape index was sensitive to the area

Table 2. Error Matrices for the MLC Method and Hybrid Method Combining Object- and Knowledge-Based Classifications (OBKB)[1]

MLC Method			
Classified as:	Non-dead	Dead	User's
Non-dead	56	9	0.862
Dead	10	66	0.868
Producer's'	0.848	0.880	
		Overall	0.865
		Kappa	0.729
OBKB Method			
Classified as:	Non-dead	Dead	User's
Non-dead	63	2	0.969
Dead	3	73	0.961
Producer's'	0.955	0.973	
		Overall	0.965
		Kappa	0.929

[1]Level 2 classification system.

of an object and should not be used for comparisons among objects directly. We proposed a relative shape index, which corrected the effects of area and allowed for direct comparison of edge complexity for objects of different sizes. The relative shape index was also demonstrated to be effective in construing domain knowledge and filtering out misclassified dead crowns with irregular shapes.

We applied three rules to improve classification accuracies of the dead crowns. Rule 1 was used to restrict the maximum possible size of a dead crown, which successfully reduced the misclassification between dead crowns and bare areas in the upper right corner of the study area (Fig. 6A, region a). Rule 2 imposed the shape requirement for dead crowns, which exhibited a relatively compact shape in the image (Fig. 6A, region c). The last rule required that dead crowns be adjacent to vegetation, which is based on our field experience and visual inspection of the image. It successfully ruled out the misclassification of some isolated segments surrounded by bare areas (Fig. 6A, region b). Moreover, we found that the area and shape index together with spatial topology were quite effective in representing human knowledge in the detection of dead crowns in our study. For example, to remove "salt-and-pepper" effects, we combined the area and shape indices to filter out small and irregular shapes. We also applied the shape index together with spatial topology to enhance classification accuracies between dead crowns and bare areas. However, it should be noted that these rules are specifically designed for detecting dead crowns. For different applications, the rules could be different. Nevertheless, we believe that the geometric properties (e.g., area, perimeter, and shape index) and spatial topology

could be very useful in representing human knowledge, and used in constructing knowledge-based classifications.

It has been documented that humans are less capable of differentiating grey levels than are computer algorithms. Yet for high-resolution remotely sensed imagery, experienced photointrepreters often outperform computer algorithms because humans use not only spectral information but also spatial and topological information. Conventional pixel-base classifiers such as contextual classifiers, which incorporate texture and spatial structure information by using a moving window template, have been demonstrated successfully to improve the classification approaches (Gong and Howarth, 1992; Karathanassi et al., 2000; Debeir et al., 2002). However, conventional contextual classifiers have difficulty in representing more sophisticated human knowledge such as object shape, area, and topological relations (Gong and Howarth, 1990a). In this study, we developed an object-based classifier together with a knowledge-based classifier to detect dead trees. We believed that the proposed methods could provide a natural solution to approximate how humans interpret images, and offer promising alternatives for the classification of high-resolution remotely sensed images.

Two final comments need to be made about the use of high-spatial-resolution imagery in vegetation classification. First, the need for high-spatial-resolution imagery should be addressed here. Despite the increased spectral information available via such imagery, the classification process is not always straightforward. In many cases, moderate spatial resolution can provide valuable information about vegetation characteristics without the cost associated with higher spatial resolution. For example, moderate-spatial-resolution imagery integrates vegetation, soil, and understory over an entire pixel, and several researchers have shown that even subtle changes to forest structure can be discerned at resolutions much larger than that of an individual tree. In other successful approaches, spectral unmixing methods have been employed to "tease out" important characteristics of individual trees (Asner, 2004). These applications using coarser spatial resolution imagery have the advantage over their high-spatial-resolution counterparts in that, in addition to deriving meaningful information about forest stands, they do so over much larger areas than is operationally possible using most high-spatial-resolution imagery with small footprints. In our case, we needed the increased spatial resolution to identify individual trees, so that we could model local conditions for mortality, and quantify the landscape-scale pattern of mortality and disease effects.

Second, the spatial characteristics of the vegetation target being examined should be considered. Our target trees are relatively compact in shape, and in most cases spectrally distinct from their surroundings. Indeed, compact shape was a component in the classification of these objects. This work suggests to us that the use of high-spatial-resolution imagery to map individual discrete objects that are larger in size than an individual pixel might better be approached with object-based (rather than with pixel-based) methods. More research is needed to investigate whether the increases in accuracy seen here from object-based classifiers over pixel-based classifiers would be consistent in areas with more spatially heterogeneous, less discrete vegetation. Areas of continuous cover of grasslands, or wetlands, for example, where the plant individuals are smaller than a pixel in size might still benefit from pixel-based classifiers. We are investigating this idea in several wetland plant communities.

CONCLUSION

Mapping overstory tree mortality in areas affected by a new forest disease in California is important for understanding spread of the disease, and provides valuable information for decision makers seeking to control it. In this study, we used 1-meter, four-band ADAR imagery to detect the dead tree crowns. We developed a hybrid classifier that integrated an object-based with a knowledge-based classification method. We first segmented the images based on a region-growing algorithm, then applied spatial filtering and merging procedures to remove "salt-and-pepper" effects. Spectral and spatial properties extracted from objects in the segmented image were used as the basic features in the hybrid method to classify the image. We found that the area, relative shape index, and topology relations extracted from the segmented image were effective in constructing expert knowledge used to distinguish dead crowns from other ground types. As comparisons, a conventional pixel-based method (maximum likelihood method) was also applied to the same image. The results indicated the hybrid image classifier that integrates an object-based method with a knowledge-based method offered significant improvements over MLC, and helped differentiate the dead crowns from other land types. We believe that the object-based method, when combined with a knowledge-based classifier, is a promising tool to assist in mapping forest mortality using high-resolution remotely sensed imagery, and expect to utilize the method across larger areas.

ACKNOWLEDGMENTS

We thank the reviewers for their constuctive comments that helped strengthen the paper. This work was partially funded by support from a NASA New Investigator Program Award to M. Kelly and by support from the California Department of Forestry and Fire Protection. Q. Guo was also supported by the Faculty Development Award of the University of California at Merced.

REFERENCES

Arbia, G., Benedetti, R., and G. Espa, 1999, "Contextual Classification in Image Analysis: An Assessment of Accuracy of ICM," *Computational Statistics & Data Analysis,* 30:443–455.

Asner, G. P., Keller, M., Rodrigo Pereira, J., Zweede, J. C., and J. N. M. Silva, 2004, "Canopy Damage and Recovery after Selective Logging in Amazonia: Field and Satellite," *Ecological Applications*, 14:S280–S298.

Baatz, M. and A. Schape, 2000, "Multiresolution Segmentation: An Optimization Approach for High Quality Multi-scale Image Segmentation," *Angewandte Geographische Informationsverarbeitung*, 12:12–23.

Baraldi, A. and F. Parmiggiani, 1996, "Single Linkage Region Growing Algorithms Based on the Vector Degree of Match," *IEEE Transactions on Geoscience and Remote Sensing,* 34:137–148.

Bardossy, A. and L. Samaniego, 2002, "Fuzzy Rule-Based Classification of Remotely Sensed Imagery," *IEEE Transactions on Geoscience and Remote Sensing,* 40:362–374.

Benediktsson, J. and I. Kanellopoulos, 1999, "Classification of Multisource and Hyperspectral Data Based on Decision Fusion," *IEEE Transactions on Geoscience and Remote Sensing,* 37:1367–1377.

Biederman, I., 1987, "Recognition-by-Components: A Theory of Human Image Understanding," *Psychological Review*, 94:115–147.

Binaghi, E., Madella, P., Montesano, M. G., and A. Rampini, 1997, "Fuzzy Contextual Classification of Multisource Remote Sensing Images," *IEEE Transactions on Geoscience and Remote Sensing,* 35:326–340.

Boyer, M., Miller, J., Belanger, M., and E. Hare, 1988, "Senescence and Spectral Reflectance in Leaves of Northern Pin Oak (*Quercus palustris muenchh*.)," *Remote Sensing of Environment,* 25:71–87.

Brandtberg, T. and F. Walter, 1998, "Automated Delineation of Individual Tree Crowns in High Spatial Resolution Aerial Images by Multiple-Scale Analysis," *Machine Vision and Applications,* 11:64–73.

Carleer, A. P., O. Debeir, and E. Wolff, 2005, "Assessment of Very High Spatial Resolution Satellite Image Segmentations," *Photogrammetric Engineering & Remote Sensing*, 11:1285–1294.

Clark, D. B., Castro, C. S., Alvarado, L. D. A., and J. M. Read, 2004, "Quantifying Mortality of Tropical Rain Forest Trees Using High-Spatial-Resolution Satellite Data," *Ecological Letters*, 7:52–59.

Congalton, R. G. and R. A. Mead, 1983, "A Quantitative Method to Test for Consistency and Correctness in Photointerpretation," *Photogrammetric Engineering and Remote Sensing*, 49:69–74.

Cumani, A., 1991, "Edge-Detection in Multispectral Images," *Cvgip—Graphical Models and Image Processing,* 53:40–51.

Debeir, O., Van den Steen, I., Latinne, P., Van Ham, P., and E. Wolff, 2002, "Textural and Contextual Land-Cover Classification Using Single and Multiple Classifier Systems," *Photogrammetric Engineering and Remote Sensing,* 68:597–605.

ERDAS, 1999, *ERDAS Field Guide*, Atlanta, GA: ERDAS, Inc.

Everitt, J., Escobar, D., Appel, D., Riggs, W., and M. Davis, 1999, "Using Airborne Digital Imagery for Detecting Oak Wilt Disease," *Plant Disease,* 83:502–505.

Garbelotto, M., Svihra, P., and D. Rizzo, 2001, "Sudden Oak Death Syndrome Fells Three Oak Species," *California Agriculture,* 55:9–19.

Gong, P. and P. J. Howarth, 1990a, "Land Cover to Land Use Conversion: A Knowledge-Based Approach, in: *Annual Conference of American Society of Photogrammetry and Remote Sensing*, Denver, CO, pp. 447–456.

Gong, P. and P. J. Howarth, 1990b, "The Use of Structural Information for Improving Land-Cover Classification Accuracies at the Rural-Urban Fringe," *Photogrammetric Engineering and Remote Sensing,* 56:67–73.

Gong, P. and P. J. Howarth, 1992, "Frequency-Based Contextual Classification and Gray-Level Vector Reduction for Land-Use Identification," *Photogrammetric Engineering and Remote Sensing,* 58:423–437.

Harris, P. M. and S. J. Ventura, 1995, "The Integration of Geographic Data with Remotely-Sensed Imagery to Improve Classification in an Urban Area," *Photogrammetric Engineering and Remote Sensing,* 61:993–998.

Hay, G., Blaschke, T., Marceau, D., and A. Bouchard, 2003, "A Comparison of Three Image Object Methods for the Multiscale Analysis of Landscape Structure," *Journal of Photogrammetry & Remote Sensing*, 57:327–345.

Hay, G., Castilla, G., Wulder M., and J. Ruiz, 2005, "An Automated Object-Based Approach for the Multiscale Image Segmentation of Forest Scenes," *International Journal of Applied Earth Observation and Geoinformation*, 7:339–359.

Hay, G., Marceau, D., Dube, P., and A. Bouchard, 2001, "A Multiscale Framework for Landscape Analysis: Object-Specific Analysis and Upscaling," *Landscape Ecology*, 16:471–490.

Holdenrieder, O., Pautasso, M., Weisberg, P., and D. Lonsdale, 2004, "Tree Diseases and Landscape Processes: The Challenge of Landscape Pathology," *Trends in Ecology and Evolution*, 19:446–452.

Karathanassi, V., Iossifidis, C., and D. Rokos, 2000, "A Texture-Based Classification Method for Classifying Built Areas According to their Density," *International Journal of Remote Sensing,* 21:1807–1823.

Kelly, M. and R. K. Meentemeyer, 2002, "Landscape Dynamics of the Spread of Sudden Oak Death," *Photogrammetric Engineering & Remote Sensing,* 68:1001–1009.

Kelly, M., Shaari, D., Guo, Q. H., and D. S. Liu, 2004, "A Comparison of Standard and Hybrid Classifier Methods for Mapping Hardwood Mortality in Areas Affected by 'Sudden Oak Death'," *Photogrammetric Engineering & Remote Sensing,* 70:1229–1239.

Kelly, N. M. and B. A. McPherson, 2001, "Multi-scale Approaches Taken to Sudden Oak Death Monitoring," *California Agriculture,* 55:15–16.

Kermad, C. D. and K. Chehdi, 2002, "Automatic Image Segmentation System through Iterative Edge-Region Co-operation," *Image and Vision Computing,* 20:541–555.

Laliberte, A. S., Rango, A., Havstad, K. M., Paris, J. F., Beck, R. F., McNeely, R., and A. L. Gonzalez, 2004, "Object-Oriented Image Analysis for Mapping Shrub Encroachment from 1937 to 2003 in Southern New Mexico," *Remote Sensing of Environment,* 93:198–210.

Li, J. and R. M. Narayanan, 2003, "A Shape-Based Approach to Change Detection of Lakes Using Time Series Remote Sensing Images," *IEEE Transactions on Geoscience and Remote Sensing,* 41:2466–2477.

Liu, D., Kelly, M., and P. Gong, 2006, "A Spatial-Temporal Approach for Monitoring Forest Disease Dynamics Using Multi-temporal High Spatial Resolution Imagery," *Remote Sensing of Environment*, 101(2):167–180.

Martin, L. R. G. and P. J. Howarth, 1989, "Change-Detection Accuracy Assessment Using SPOT Multispectral Imagery of the Rural-Urban Fringe," *Remote Sensing of Environment,* 30:55–66.

Moghaddamzadeh, A. and N. Bourbakis, 1997, "A Fuzzy Region Growing Approach for Segmentation of Color Images," *Pattern Recognition,* 30:867–881.

Muchoney, D. M. and B. N. Haack, 1994, "Change Detection for Monitoring Forest Defoliation," *Photogrammetric Engineering & Remote Sensing,* 60:1243–1251.

Mumby, P. J. and A. J. Edwards, 2002, "Mapping Marine Environments with IKONOS Imagery: Enhanced Spatial Resolution Can Deliver Greater Thematic Accuracy," *Remote Sensing of Environment,* 82:248–257.

Murai, H. and S. Omatu, 1997, "Remote Sensing Image Analysis Using a Neural Nnetwork and Knowledge-Based Processing," *International Journal of Remote Sensing,* 18:811–828.

Pal, N. R. and S. K. Pal, 1993, "A Review on Image Segmentation Techniques," *Pattern Recognition,* 26: 1277–1294.

Read, J. M., 2003, "Spatial Analyses of Logging Impacts in Amazonia Using Remotely Sensed Data," *Photogrammetric Engineering and Remote Sensing*, 69: 275–282.

Richards, J. and X. Jia, 1999, *Remote Sensing Digital Image Analysis: An Introduction,* New York, NY: Springer-Verlag.

Rizzo, D. M. and M. Garbelotto, 2003, "Sudden Oak Death: Endangering California and Oregon Forest Ecosystems," *Frontiers in Ecology and the Environment,* 1:197–204.

Rizzo, D., Garbelotto, M., Davidson, J. M., Slaughter, G. W. and S. T. Koike, 2002, "*Phytophthora ramorum* as the Cause of Extensive Mortality of *Quercus* spp. and *Lithocarpus densiflorus* in California," *Plant Disease,* 86:205–213.

Sali, E. and H. Wolfson, 1992, "Texture Classification in Aerial Photographs and Satellite Data," *International Journal of Remote Sensing,* 13:3395–3408.

Sarabi, A. and J. K. Aggarwal, 1981, "Segmentation of Chromatic Images," *Pattern Recognition,* 13: 417–427.

Solberg, A. H. S., 1999, "Contextual Data Fusion Applied to Forest Map Revision," *IEEE Transactions on Geoscience and Remote Sensing,* 37:1234–1243.

Steele, B. M. and R. L. Redmond, 2001, "A Method of Exploiting Spatial Information for Improving Classification Rules: Application to the Construction of Polygon-Based Land Cover Maps," *International Journal of Remote Sensing,* 22:3143–3166.

Stefanov, W. L., Ramsey, M. S. and P. R. Christensen, 2001, "Monitoring Urban Land Cover Change: An Expert System Approach to Land Cover Classification of Semiarid to Arid Urban Centers," *Remote Sensing of Environment,* 77:173–185.

Svihra, P., 1999, "Tanoak and Coast Live Oak under Attack," *Oaks 'n' Folks,* 14:1.

Toll, D. L., 1984, "An Evaluation of Simulated Thematic Mapper Data and Landsat MSS Data for Discriminating Suburban and Regional Land Use and Land Cover," *Photogrammetric Engineering & Remote Sensing,* 50:1713–1724.

Tonjes, R., Growe, S., Buckner, J. and C. E. Liedtke, 1999, "Knowledge-Based Interpretation of Remote Sensing Images Using Semantic Nets," *Photogrammetric Engineering and Remote Sensing,* 65:811–821.

Treitz, P. M., Howarth, P. J., Suffling, R. C. and P. Smith, 1992, "Application of Detailed Ground Information to Vegetation Mapping with High Spatial-Resolution Digital Imagery," *Remote Sensing of Environment,* 42:65–82.

Tremeau, A. and N. Borel, 1997, "A Region Growing and Merging Algorithm to Color Segmentation," *Pattern Recognition,* 30:1191–1203.

Xia, L., 1996, "A Method to Improve Classification with Shape Information," *International Journal of Remote Sensing,* 17:1473–1481.

Zhang, Y. J., "Evaluation and Comparison of Different Segmentation Algorithms," *Pattern Recognition Letters*, 18:963–974.

Zhang, Y. J. and J. J. Gerbrands, 1994, "Objective and Quantitative Segmentation Evaluation and Comparison," *Signal Processing,* 39:43–54.

Zhang, Y. J. and H. T. Luo, 2000, "Optimal Selection of Segmentation Algorithms Based on Performance Evaluation," *Optical Engineering,* 39:1450–1456.